Contents lists available at ScienceDirect

Arabian Journal of Chemistry

journal homepage: www.ksu.edu.sa

Original article

Preparation of three kinds of efficient sludge-derived adsorbents for metal ions and organic wastewater purification

Hui Guo [a], Song Cheng [b,c,*], Baolin Xing [b,c,*], Mingliang Meng [b], Laihong Feng [d], Yanhe Nie [b], Chuanxiang Zhang [b]

[a] School of Materials Science and Engineering, Henan Polytechnic University, Jiaozuo 454003, China
[b] College of Chemistry and Chemical Engineering, Henan Polytechnic University, Jiaozuo 454003, China
[c] Collaborative Innovation Center of Coal Work Safety and Clean High Efficiency Utilization, Jiaozuo 454003, China
[d] Huaneng Coal Technology Research Co., Ltd., Beijing 100070, China

ARTICLE INFO

Keywords:
MgAl-LDO
Sludge
Sludge activated carbon
Sludge ceramsite
Wastewater treatment

ABSTRACT

The sludge is pretreated to prepare the sludge bicohar by pyrolysis, which is divided into high-carbon sludge biochar and high-ash sludge biochar using flotation. The high-carbon sludge biochar and high-ash sludge biochar are used to prepare the sludge activated carbon, MgAl-layered double hydroxides (MgAl-LDO) and sludge ceramsite for Pb^{2+}, methyl orange (MO) and ciprofloxacin (CIP) removal from wastewater, respectively. The sludge activated carbon is prepared from high-carbon sludge biochar using $ZnCl_2$ as chemical agent in the additive of pine sawdust for MO and CIP removal with adsorption amount of the 754.05 mg/g and 635.62 mg/g, respectively. Mg-Al LDO is prepared from the leaching solution of the high-ash sludge bicohar, which can quickly remove Pb^{2+} from wastewater with adsorption amount of 147.89 mg/g. Mg-Al LDO has good reusability after three cycles. The MO/CIP and Pb^{2+} adsorption mechanism are analyzed and investigated. The sludge ceramsite prepared from the leaching residue of high-ash sludge bicohar is also used for Pb^{2+} removal. The above results indicate that sludge is converted into three kinds of the adsorbents for pollution removal from wastewater.

1. Introduction

Water pollution has caused global concern owe to its destruction of ecological environment (Yuan et al., 2023; Zhao et al., 2023). The Pb^{2+}, organic dye and antibiotic wastewater are great harm to the human beings and aquatic life (Cheng et al., 2021b; Wang et al., 2022). These pollutants are not easy non-degradable in the wastewater (Wang et al., 2022a; Le et al., 2023). Pb^{2+} can seriously damage the nervous system, physiological systems and other organs (Cheng et al., 2021a). The organic dye will increase the chroma of receiving water, which prevents the photosynthesis in plants (Foroutan et al., 2022). The antibiotics are the organic compounds, which is one of the emerging contaminants in wastewater (Foroutan et al., 2021). Antibiotics can produce the resistant bacteria and resistance genes, which have seriously threatened to the human beings (Omer et al., 2022). These pollutions can easily migrate and accumulate in wastewater, posing a great threat to human and environment (Chakraborty et al., 2020).

The treatment methods of wastewater include chemical precipitation (Benalia et al., 2021), ion exchange (Dabrowski et al., 2004), membrane division (Li et al., 2009), adsorption (Ran et al., 2022) and phytoremediation (Awa & Hadibarata, 2020). The adsorption technology is considered as the suitable and effective treatment method among these treatment method owe to good adsorption efficiency and easy operation (Yurak et al., 2021; Zhou et al., 2022). Qin et al. (2024) prepared ZnO decorated biochar for levofloxacin removal from wastewater with adsorption capacity of 193.42 mg/g. Cheng et al., (2021a) prepared the modification crofton weed for Pb^{2+} removal from wastewater with the adsorption capacity of 234.60 mg/g. Cheng et al., (2022b) reported that the rhodamine B and malachite green adsorption capacities of magnetic separation photocatalyst-adsorbent are 475.49 mg/g and 646.82 mg/g, respectively. However, the price of the common adsorbent is expensive. Therefore, it is necessary to prepare the adsorbent with high adsorption capacity and low cost in practical engineering.

Preparation of high efficiency and low-cost adsorbent has attracted the attention of the researchers for pollutant removal (Wang et al., 2022b; Zhang et al., 2023). The published literatures have reported various of adsorbents prepared form various of wastes such as agricultural and sidelong products, sludge and other solids waste (Florent et al.,

* Corresponding authors.
E-mail addresses: cskmust@163.com (S. Cheng), baolinxing@hpu.edu.cn (B. Xing).

https://doi.org/10.1016/j.arabjc.2024.105671
Received 11 November 2023; Accepted 7 February 2024
Available online 10 February 2024

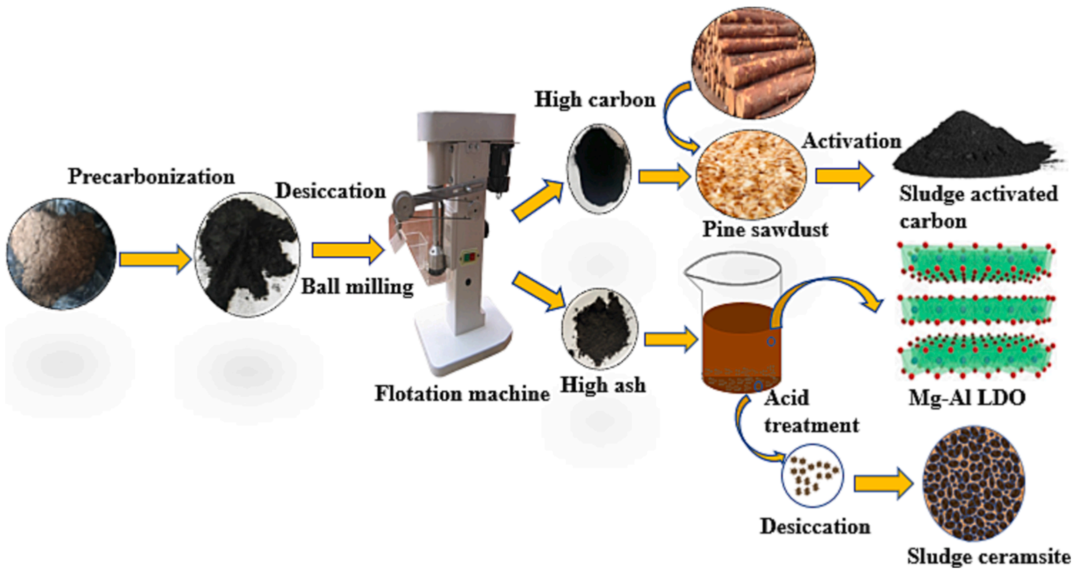

Fig. 1. Schematic diagram of sludge separation process.

2019; Vázquez-Durán et al., 2022). Lee et al. (2019) used the ginkgo biloba leaves as the raw material to prepare the adsorbent for Pb(II) and Cu(II) removal with good removal, respectively. The sewage sludge is the by-product of wastewater biological treatment, which is also kind of municipal solid waste. Hu et al. (2022) reported that sludge production is about 45 million every year. The sludge has many harmful substances such as heavy metals and harmful organic matter. Therefore, it should find an environmentally-friendly method to utilize the sludge to avoid polluting environment. Cheng et al., (2021c) used sludge to prepare the $ZnCl_2$-$FeCl_3$ modified sludge for methyl orange removal from wastewater with good result. Yan et al. (2022) reported that sludge-coconut fiber biochar can efficiently remove the ciprofloxacin, Zn and Cd from wastewater. Ma et al. (2020) prepared the modified sludge-derived biochar for CIP, norfloxacin and ofloxacin removal from wastewater with large adsorption capacity. Liu et al. (2021) used the NaOH-modified sludge to remove tetracycline from wastewater with the adsorption amount of 379.78 mg/g. Therefore, sludge can be used as the feedstock to prepare high efficient adsorbent for pollutions removal.

Pyrolysis is a common method for pretreatment of sludge. Biochar obtained from sludge pyrolysis can be used as the adsorbent for organic and inorganic pollutants removal. However, sludge has lots of inorganic mineral salt (Al_2O_3, Fe_2O_3 and SiO_2), which limit its application in wastewater treatment. Therefore, the sludge biochar should be pretreated to remove the inorganic mineral salts before use. The flotation is a kind of methods for purification of minerals, which can be used to purify the sludge biochar. The sludge biochar can be divided into the high-ash sludge biochar and high-carbon sludge biochar after flotation. The high ash sludge biochar contains bivalent, trivalent metal cations and multiple anions such as calcium, aluminum, iron and magnesium, which can be used as the feedstock to prepare the layered double hydroxides (Jawad et al., 2018). The high-carbon sludge biochar can be used to prepare the sludge active carbon for pollutants removal from wastewater. The adsorbents prepared from sludge can be used in wastewater treatment.

In this work, sludge is used to prepare the sludge biochar by pyrolysis, which is divided into the high-carbon sludge biochar and high-ash sludge biochar using flotation. The high-carbon sludge biochar is used to prepare the sludge activated carbon using $ZnCl_2$ as chemical agent to extend the pore structure of the sludge activated carbon. Mg-Al LDO is prepared from the leaching solution of the high-ash sludge bicohar. Besides, leaching residue of high-ash sludge biochar is used as the feedstock to prepare the sludge ceramsite. The innovation of this research is that the sludge is totally converted into three kinds of adsorbents, realizing the zero-emission of the sludge and avoiding the environment pollution caused from the sludge. The Pb^{2+}, CIP and MO are used the pollution model to investigate the adsorption performance of the prepared adsorbent. The main objectives of this work are to: (1) investigate the physicochemical properties of prepared adsorbent, (2) analyze the adsorption performance of prepared adsorbent, (3) analyze the involved in adsorption mechanism of the pollution. This research work will achieve the high-value use of the sludge.

2. Experimental

2.1. Sludge separation and utilization

The sludge is pretreated by pyrolysis to obtain the sludge biochar at 600 °C for 2 h. The sludge biochar can be divided into the high-carbon sludge biochar and high-ash sludge biochar after flotation. The high-carbon sludge biochar is mixed with pine sawdust to prepare the sludge activated carbon using $ZnCl_2$ as chemical agent. The high-ash sludge biochar can be divided into the leaching solution and leaching residue after acid-leaching treatment. The leaching solution is used as feedstock to prepare the Mg-Al LDO in the existence of the adjusting reagent (Qu et al., 2023a). The leaching residue is mixed with the coal gangue and other auxiliary materials to prepare sludge ceramsite at high temperature. The utilization process of sludge is shown in Fig. 1.

2.2. Preparation of adsorbent derived from sludge

2.2.1. Preparation of sludge activated carbon

10 g high-carbon sludge biochar is mixed with 10 g pine sawdust in the 200 mL distilled water. Besides, 30 g $ZnCl_2$ is added into the above mixed solution, which is stirred for 24 h. After that, the mixture is heated in the tube furnace (Song et al., 2023). The heat temperature and heat time are 500 °C and 60 min, respectively. The residue in the tube furnace is named as the sludge activated carbon.

2.2.2. Preparation of MgAl-LDO

4.8 g NaOH and 12.72 g Na_2CO_3 are mixed in the 500 mL deionized water to prepare the mixed alkali solution. $MgCl_2$ is added into high-ash sludge biochar soaked in hydrochloric acid. And then 500 mL deionized water is added to prepare the mixed salt solution. The two mixtures are mixed into the beaker, which is continuously stirred at a rotating speed

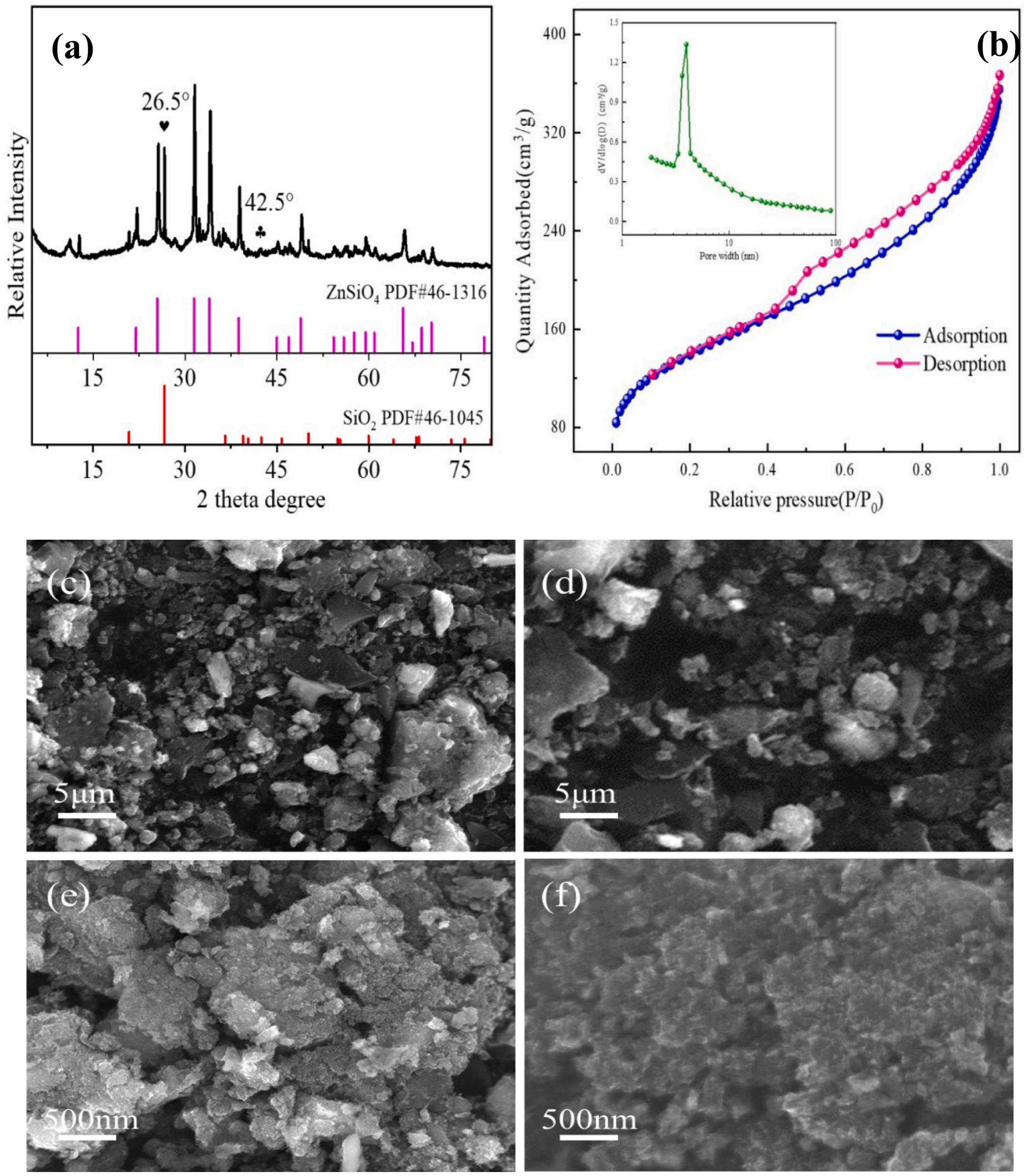

Fig. 2. XRD spectrum analysis of the sludge activated carbon (a), N_2 adsorption isotherm of pore distribution of the sludge activated carbon (b), and SEM images of the sludge (c–d) and sludge activated carbon (e–f).

of 180 r/min for 30 min. Then the mixture is placed into the three-mouth flask at 60 °C. Finally, the mixture is filtered and washed, which is dried in a vacuum drying oven at 105 °C. The dried sample is named as the MgAl-LDH. After that, MgAl-LDH is heated in the muffle furnace at 500 °C for 2 h, which is named as the MgAl-LDO (Qu et al., 2023b).

2.2.3. Preparation of sludge ceramsite

The leaching residue after acid leaching of high-ash sludge biochar is dried and crushed, which is pretreated using ball mill for 8 h at a rotating speed of 180 r/min. And then the mass ratio of the leaching residue: coal gangue: kaolin: coal powder: glass powder is 6:1:1:1:1, which is mixed evenly. The mixture is added into the granulator. The prepared pellets are uniformly placed on the iron plate and dried at 105 °C for 2 h. Dried raw pellets are pushed into the muffle furnace at 1200 °C for 10 min. The residue in the muffle furnace is the sludge ceramsite. The detailed information of the adsorption experiment is in the supporting information.

2.3. Characterizations

The surface microstructure of sample is investigated using scanning electron microscopy (SEM) (SEM, Philips XL30ESEM-TMP). The composition of the sample is analyzed by X-ray diffraction (XRD) (D/max-3B, Japan) (Zeng et al., 2023). Surface chemical properties of sample are detected by X-ray photoelectron spectroscopy (XPS) (Physical Electronics, Inc., Chanhassen, MN, USA) (Shi et al., 2024). The surface functional groups of samples are analyzed using the Fourier transform infrared spectroscopy (FTIR) (Thermo Fisher Scientific, USA).

3. Results and discussion

3.1. Characterization of sludge activated carbon and its application

3.1.1. Characterization of sludge activated carbon

Fig. 2a shows the XRD spectrum analysis of the sludge activated carbon. As Fig. 2a shown, the sludge activated carbon has the peaks of inorganic substances. The peaks of SiO_2 at 26.5° and 42.5° are appeared

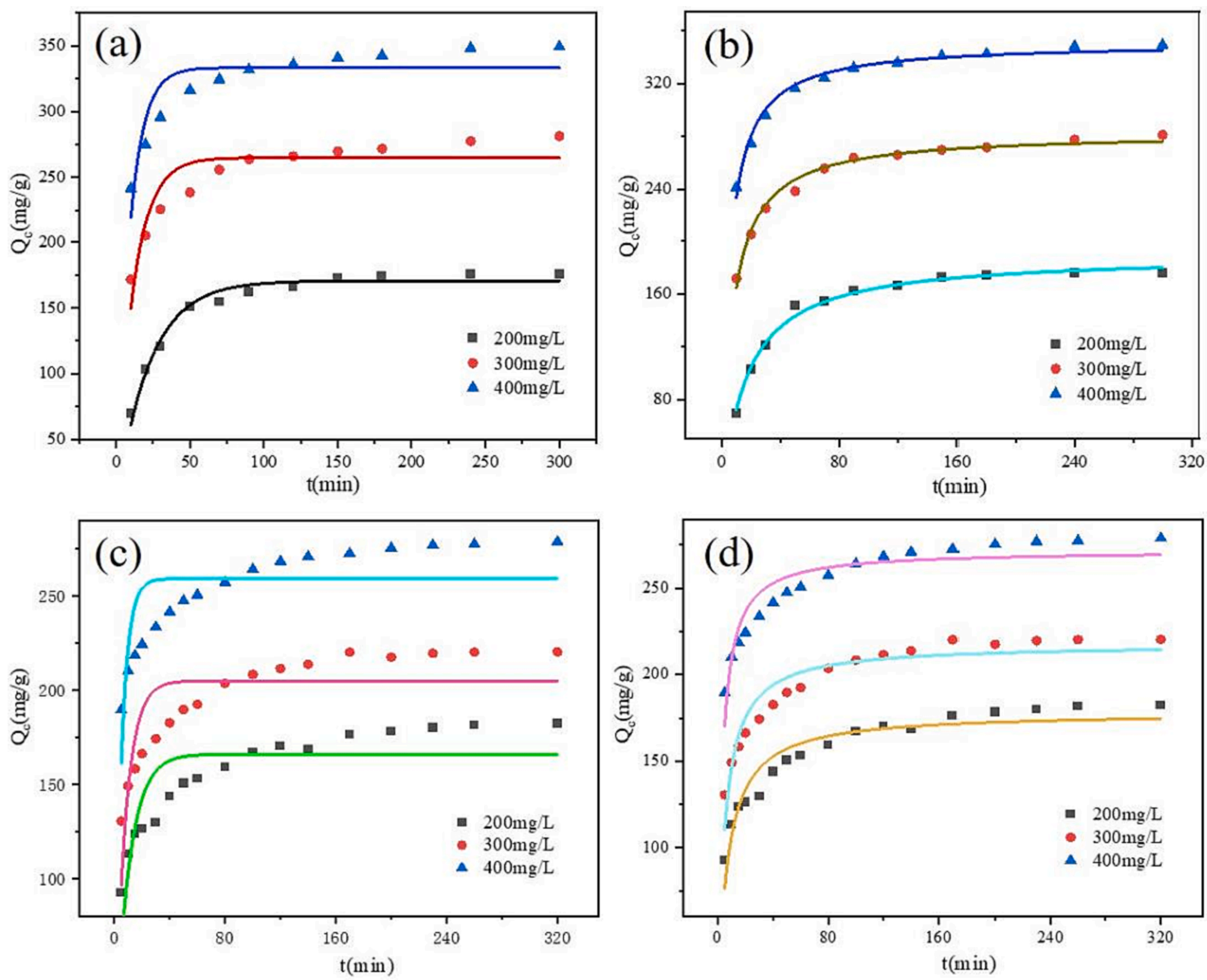

Fig. 3. MO (a) and CIP (c) adsorption data fitting Pseudo-first-order kinetics, and MO (b) and CIP (d) adsorption data fitting Pseudo-second-order kinetics model.

Table 1
The fitting results of MO and CIP adsorption data fitting the adsorption kinetics model.

Pollution	Model	Parameters	Initial concentration (mg/L)		
			200	300	400
MO	Pseudo-first-order	R^2	0.977	0.837	0.796
		k_1	0.044	0.082	0.106
		$Q_{e,c}$ (mg/g)	170.61	264.93	333.30
	Pseudo-second-order	R^2	0.991	0.985	0.986
		k_2	0.032	0.007	0.014
		$Q_{e,c}$ (mg/g)	189.54	282.87	351.09
CIP	Pseudo-first-order	R^2	0.689	0.639	0.541
		k_1	0.097	0.126	0.191
		$Q_{e,c}$ (mg/g)	166.01	205.01	259.27
	Pseudo-second-order	R^2	0.911	0.925	0.897
		k_2	0.008	0.009	0.001
		$Q_{e,c}$ (mg/g)	178.24	217.68	271.82

Table 2
The fitting results of MO and CIP adsorption data fitting adsorption isotherm model.

Pollution	Isotherms	Parameters	Temperature (°C)		
			30	40	50
MO	Langmuir	R^2	0.993	0.993	0.990
		Q_{max} (mg/g)	726.57	745.65	754.05
	Freundlich	R^2	0.986	0.987	0.986
		n	0.661	0.63369	0.618
		k_F	6.800	8.481	9.446
CIP	Langmuir	R^2	0.983	0.981	0.984
		Q_{max} (mg/g)	618.37	624.32	635.62
	Freundlich	R^2	0.967	0.982	0.978
		n	0.446	0.434	0.430
		k_F	19.854	22.148	22.863

on sludge activated carbon. Besides, the strong diffraction peak of zinc silicate is also found on sludge activated carbon. Fig. 2b shows the N_2 adsorption isotherm of sludge activated carbon. As Fig. 2b shown, the type of adsorption isotherm belongs to H_2 hysteresis loop, which gradually increases in the low pressure with few micropores. The curve slope of the adsorption isotherm quickly increases at $P/PO \geq 0.5$, indicating that the mesoporous percentage is high (Cheng et al., 2022a). The special surface area of the sludge activated carbon is 480.18 m^2/g.

Fig. 2c–f shows the SEM images of the sludge and sludge activated carbon. The sludge activated carbon has fibrous and irregular pore structure, forming many irregular protrusions compared to sludge. This result is similar to the "sponge" wrapped around sludge activated carbon. $ZnCl_2$ is a kind of the chemical agent to extend the pore structure of

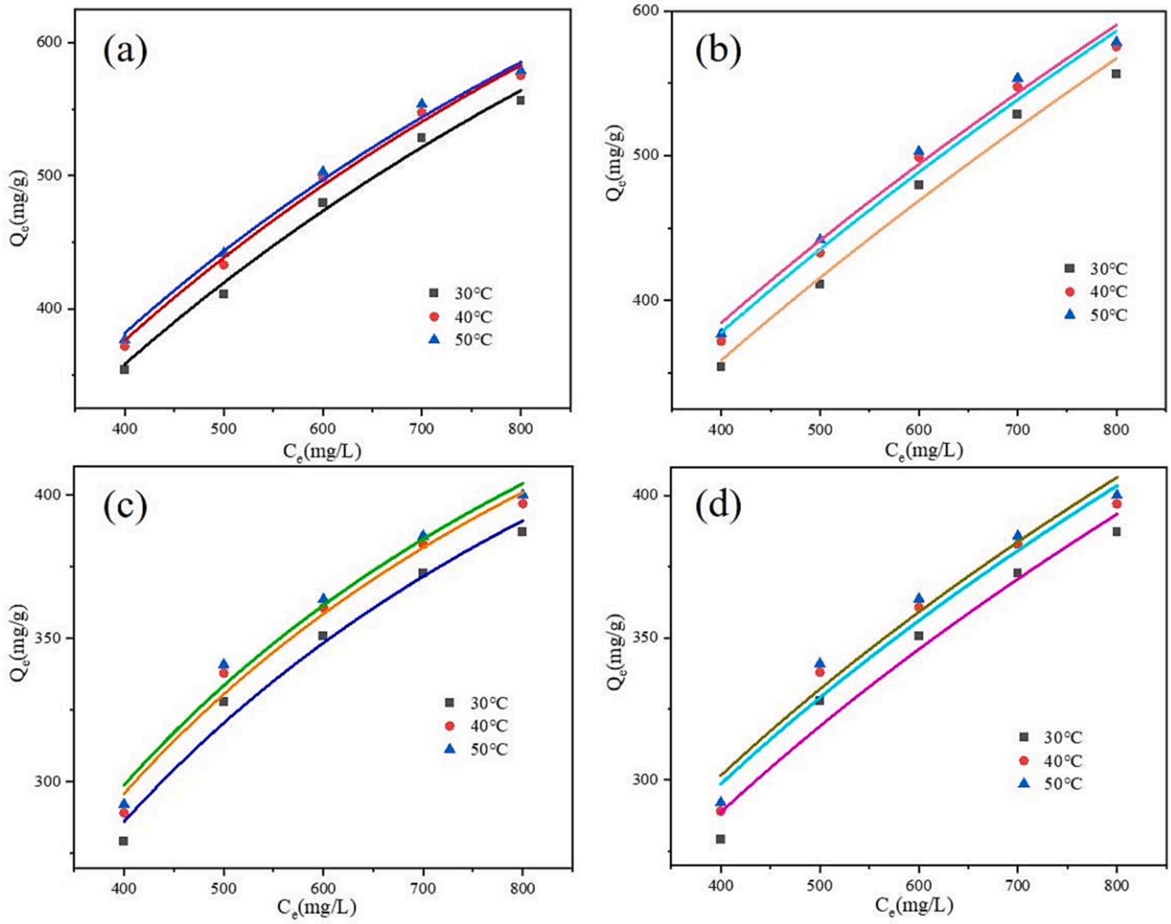

Fig. 4. MO (a) and CIP (c) adsorption data fitting the Langmuir model, and MO (b) and CIP (d) adsorption data the Freundlich model.

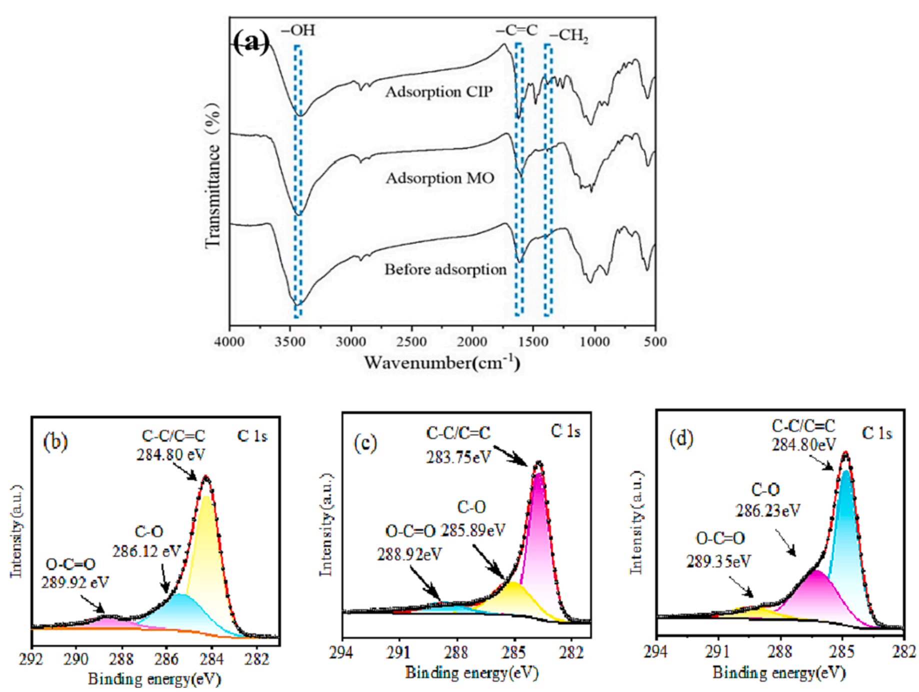

Fig. 5. FT-IR spectra (a) and C1s spectra analysis of before (b) and after MO (c) and CIP (d) adsorption of sludge activated carbon.

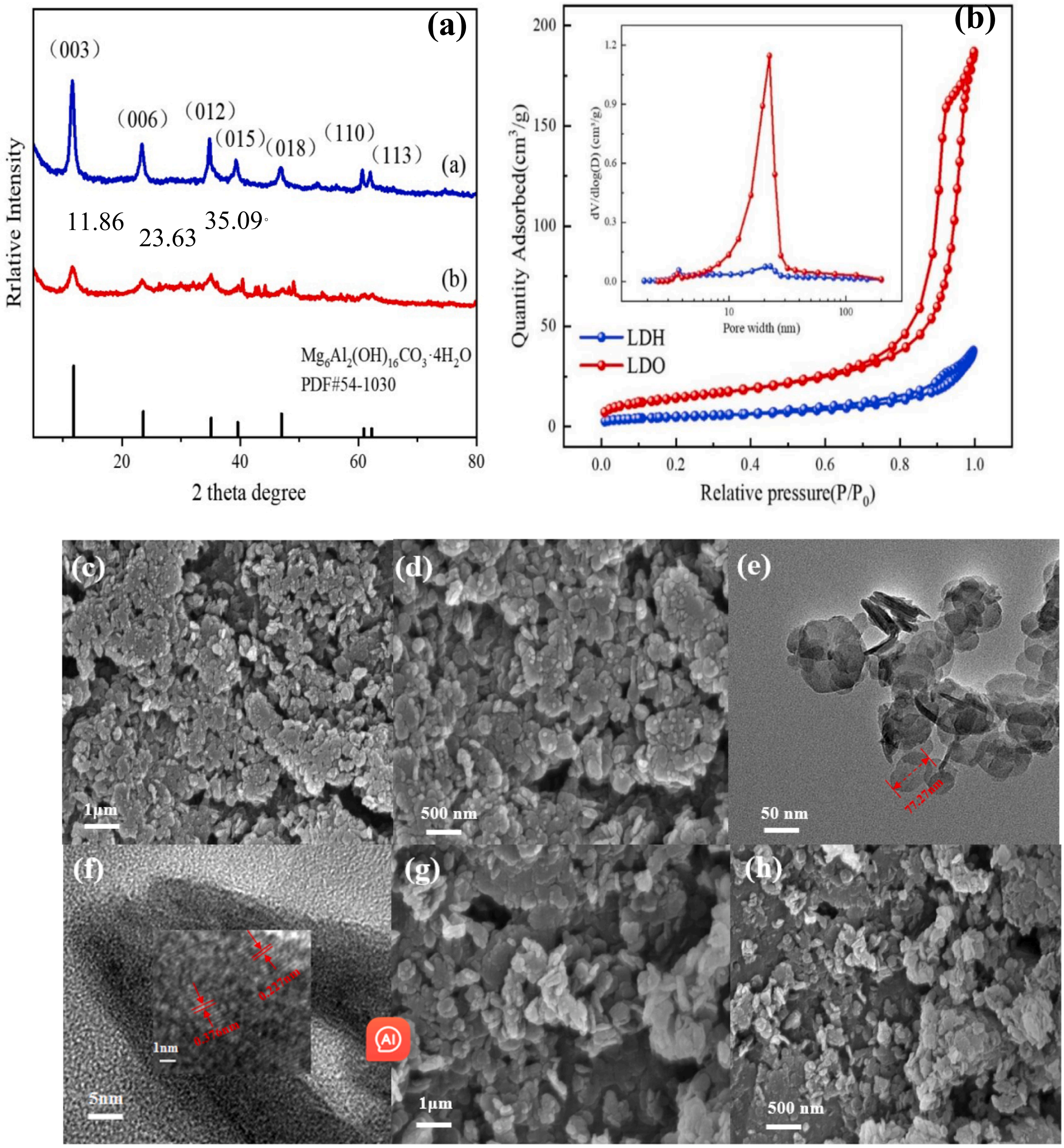

Fig. 6. XRD spectra of MgAl-LDH and MgAl-LDO (a), N_2 adsorption–desorption isotherms and pore size distribution curves of MgAl-LDH and MgAl-LDH (b), SEM (c–d) and TEM (e–f) images of MgAl-LDH, and SEM (g–h) images of MgAl-LDO.

Table 3
Fitting results of Pb^{2+} adsorption data fitting the adsorption kinetics model.

Model	Parameters	Initial concentration (mg/L)		
		200	300	400
Pseudo-first-order	R^2	0.981	0.982	0.982
	k_1	0.006	0.008	0.012
	$Q_{e,c}$ (mg/g)	133.17	142.97	150.15
Pseudo-second-order	R^2	0.984	0.985	0.986
	k_2	0.001	0.001	0.001
	$Q_{e,c}$ (mg/g)	195.74	195.99	181.82

sludge activated carbon in the preparation process. The surface of sludge activated carbon becomes loose and forms a certain of pore after $ZnCl_2$ activation, which contributes to pollutions removal from wastewater.

3.1.2. MO and CIP adsorption on sludge activated carbon

3.1.2.1. MO and CIP adsorption kinetics. Pseudo-first-order and pseudo-second-order kinetic model are used to analyze MO and CIP adsorption process (Cheng et al., 2022b). As Fig. 3 shown, MO and CIP removal quickly increase at the beginning, and then gradually reach adsorption equilibrium. Table 1 lists the fitting results of MO and CIP adsorption data fitting adsorption kinetics models. As Table 1 shown, the correlation coefficient R^2 of the pseudo-second-order kinetic is larger than the pseudo-first-order at 200–400 mg/L, indicating that pseudo-second-order kinetic can accurately describe MO and CIP adsorption process.

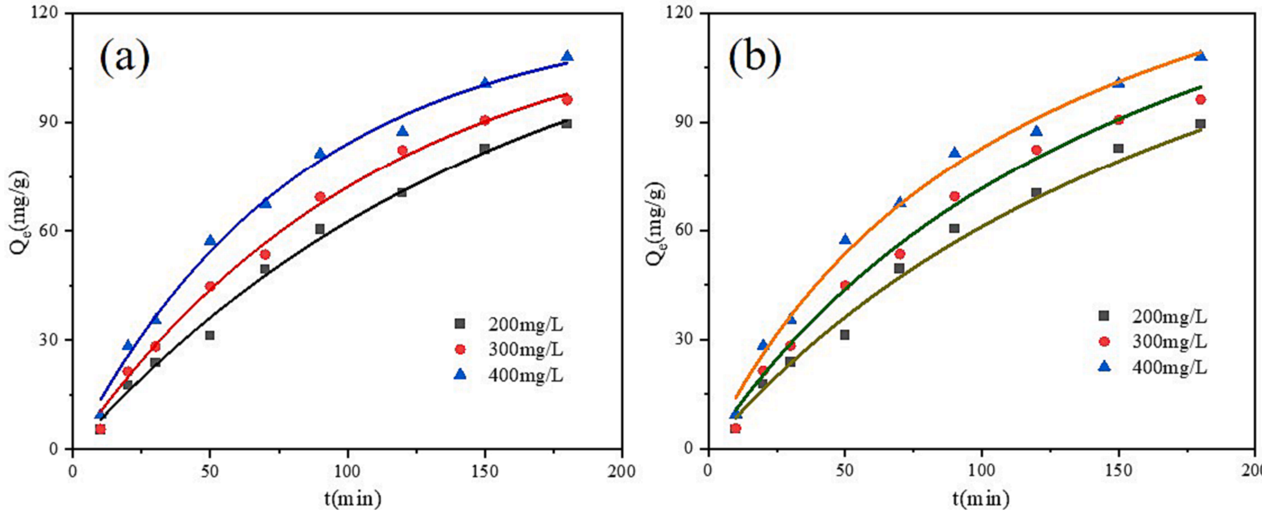

Fig. 7. Pb^{2+} adsorption data fitting the Pseudo-first-order kinetics (a) and Pseudo-second-order kinetics (b) models.

Table 4
Fitting parameters of Pb^{2+}adsorption data fitting adsorption isotherm model.

Model	Parameters	Temperature (°C)		
		30	40	50
Langmuir	R^2	0.975	0.979	0.987
	Q_{max} (mg/g)	147.89	153.96	172.7
	k_L	0.006	0.008	0.007
Freundlich	R^2	0.997	0.995	0.991
	n	0.337	0.288	0.329
	k_F	0.847	0.503	0.849

This result indicates that MO and CIP adsorption process belong to the chemical adsorption. The efficiency of adsorption system is related to the adsorption site of the sludge activated carbon (Li et al., 2022a). It does not depend on the concentration of MO and CIP in the solution.

3.1.2.2. MO and CIP adsorption isotherm. MO and CIP adsorption process are further analyzed using the Langmuir and Freundlich isotherm models. Table 2 lists the fitting results. As Table 2 shown, MO and CIP adsorption on sludge activated carbon conform to the Langmuir and Freundlich adsorption isotherm model. However, the R^2 values of MO and CIP adsorption data fitting the Langmuir model are large compared to the Freundlich model, indicating that Langmuir model is more consistent with MO and CIP adsorption process. As Table 2 shown, MO and CIP adsorption amount are increase as adsorption temperature increases. This result indicates that MO and CIP adsorption on sludge activated carbon are endothermic process. Therefore, MO and CIP adsorption amount of sludge activated carbon could be improved by increase of the adsorption temperature in the actual adsorption process. As Table 2 shown, the MO and CIP adsorption amount of the sludge activated carbon are 754.05 and 635.62 mg/g, respectively, according to Langmuir model calculation. Fig. 4 shows the MO and CIP adsorption data fitting the Langmuir and Freundlich adsorption isotherm models. As Fig. 4 shown, MO and CIP adsorption amount gradually increase until adsorption equilibrium as MO and CIP concentration increase at different adsorption temperature. Table S3 lists the adsorption capacity of similar adsorbents for MO and CIP removal from wastewater. The comparison result indicates that sludge activated carbon has promising potential in MO and CIP wastewater treatment.

3.1.2.3. Adsorption mechanism. FT-IR spectra of the sludge activated carbon before and after MO and CIP adsorption are shown in Fig. 5a. As Fig. 5a shown, the peaks of the 3420, 2925 and 1626 cm^{-1} correspond to the —OH stretching vibration peak, C—H stretching vibration and C═C stretching vibration, respectively. The peak position of the C═C stretching vibration peak has changed to the 1605 cm^{-1} after MO adsorption. This result indicates that it exists the π-π conjugate reaction between sludge activated carbon and benzene ring of MO. The fluorine in CIP molecule has a strong ability of electron absorption, which can bond with C atom. Therefore, it can be acted as the π-electron acceptor to form the π-π accumulation with aromatic C═C. Besides, surface

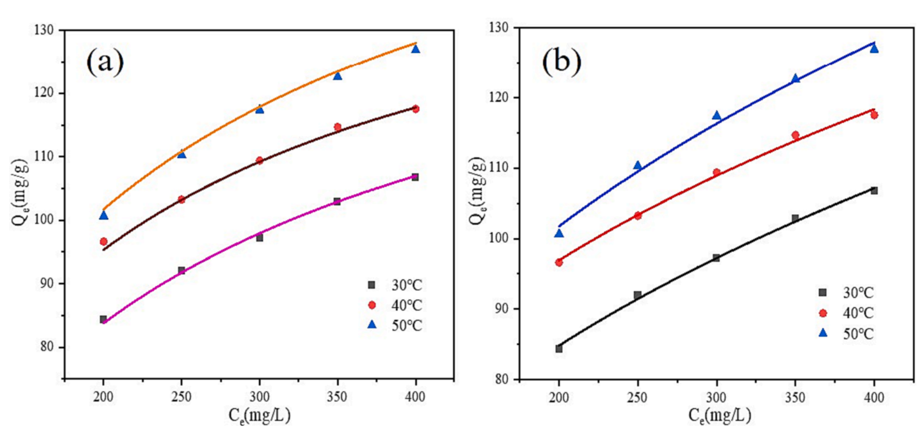

Fig. 8. Pb^{2+} adsorption data fitting the Langmuir (a) and Freundlich (b) models.

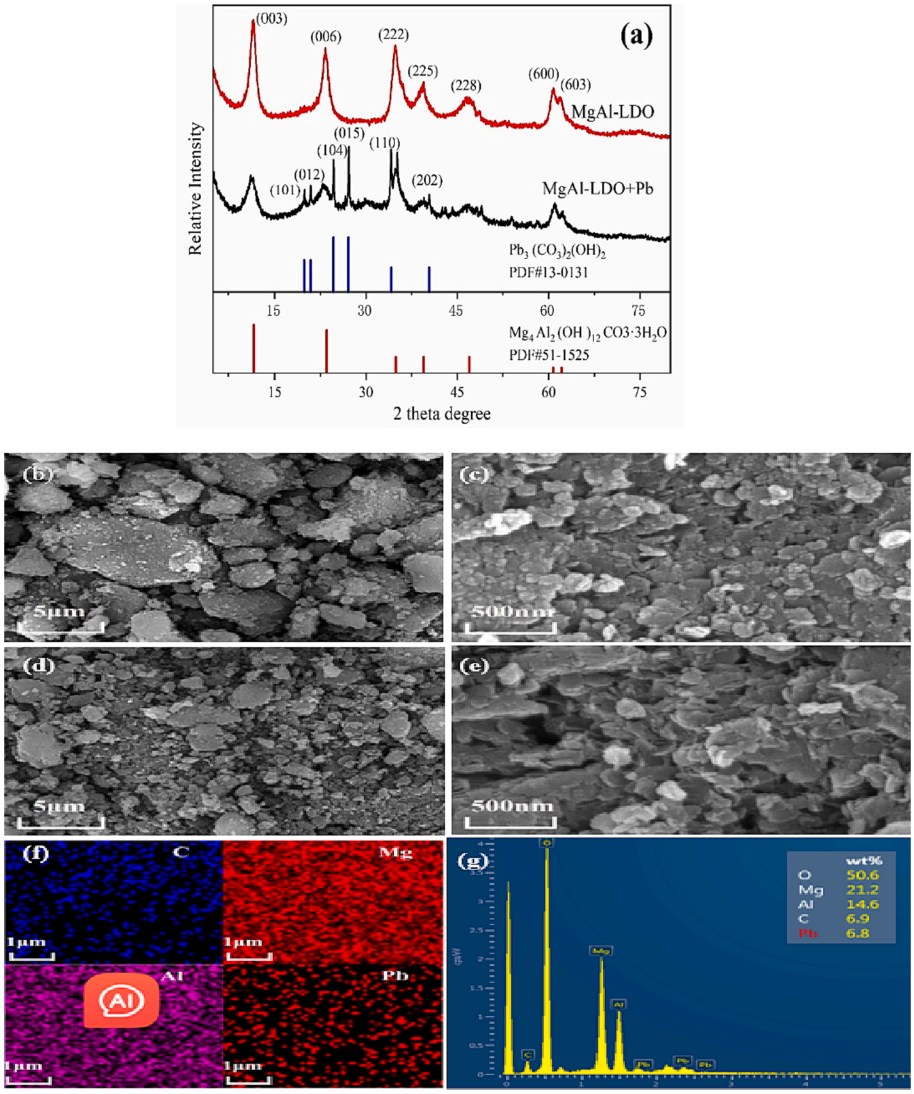

Fig. 9. The XRD spectra of MgAl-LDO before and after Pb^{2+} adsorption (a), SEM images of MgAl-LDO (b–c) and Pb^{2+} adsorption on MgAl-LDO (d–e) and EDS images of the Pb^{2+} adsorption on MgAl-LDO (f–g).

chemical groups such as C═O and —OH can also bind with MO and CIP, realizing MO and CIP removal from wastewater.

C1s spectra analysis of the sludge activated carbon before (a) and after MO (b) and CIP (c) adsorption are shown in Fig. 5b. C1s spectrum has three peaks, which are O—C═O, C—O and C—C/C═C group, corresponding to the binding energies of the 289.92 eV, 286.12 eV and 284.80 eV, respectively. O—C═O/C—O peak area decrease by 0.43 % and 2.20 % after MO adsorption, respectively. While, O—C═O peak area also decreases after CIP adsorption. This result indicates that O—C═O/C—O group involve in MO and CIP adsorption.

Sludge activated carbon has well-developed pore structure, which also contributes to MO and CIP adsorption. In summary, the adsorption mechanism of MO and CIP includes physical adsorption of pore in the sludge activated carbon, π-π conjugate reaction and surface functional groups complexation.

3.2. Characterization of MgAl-LDO and its application

3.2.1. Characterization of MgAl-LDO

XRD spectra of the MgAl-LDH and MgAl-LDO are shown in Fig. 6a. As Fig. 6a shown, the characteristic diffraction peaks of the MgAl-LDH are obvious appeared at peak of the 11.86°, 23.63° and 35.09°. This result indicates that MgAl-LDH is successfully prepared using the leaching solution of high-ash sludge bicohar. Characteristic diffraction peak of the MgAl-LDH is similar with the MgAl-LDO. N_2 adsorption isotherm analysis of the MgAl-LDO and MgAl-LDH is shown in Fig. 6b. The adsorption isotherm curve is the typical of non-rigid aggregates of H_3 type. The specific surface area of the MgAl-LDH and MgAl-LDO is 17.59 m^2/g and 52.31 m^2/g, respectively. The specific surface area of the MgAl-LDO increases after heat treatment. MgAl-LDO has large specific surface area, contributing to pollutants removal.

Fig. 6c–h shows SEM-TEM images of the MgAl-LDH and MgAl-LDO. As Fig. 6c–d shown, MgAl-LDH has good morphology with the platelet-like nanosheet structure. The lamellar structure of the MgAl-LDH stacks tight with the uniform structure, indicating that MgAl-LDH has high purity. Fig. 6e shows the cross-section of MgAl-LDH with the diameter of 77.27 nm. The fringe widths of MgAl-LDH are 0.376 nm and 0.227 nm, which are consistent with the peaks (006) and (015) of PDF#54-1030 of MgAl-LDH standard card, respectively (Khatem et al., 2015). As Fig. 6g–h shown, MgAl-LDO appears the irregular polygon structure after heat treatment.

3.2.2. Pb^{2+} adsorption on MgAl-LDO

3.2.2.1. Pb^{2+} adsorption kinetics. Pb^{2+} adsorption kinetics process is

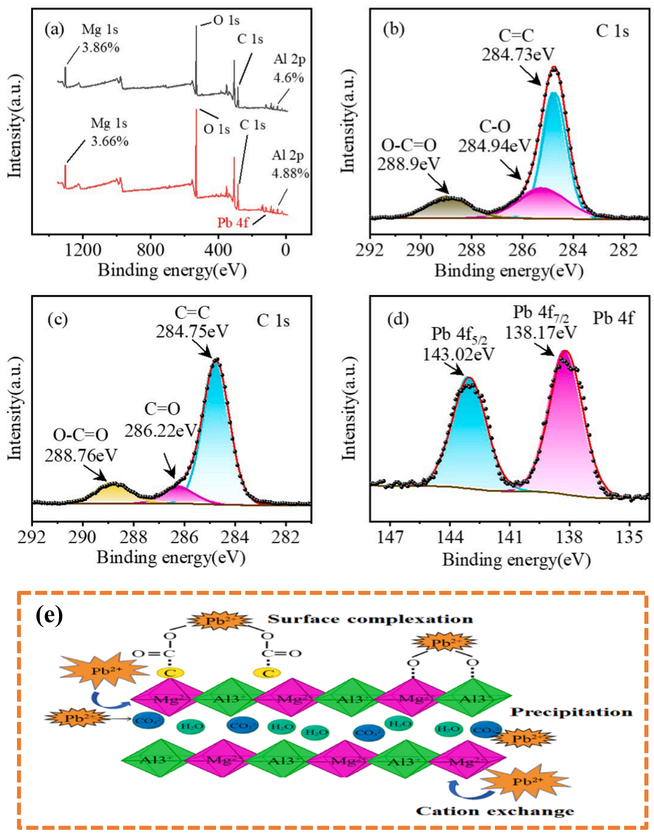

Fig. 10. XPS scan spectrum (a) and C1s XPS spectra of MgAl-LDO before and after Pb^{2+} adsorption (b-d) and Pb4f of MgAl-LDO after Pb^{2+} adsorption (e).

further analyzed using the pseudo-first-order and pseudo-second-order model (Shi et al., 2021). The fitting results of Pb^{2+} adsorption on MgAl-LDO are listed in Table 3. Pb^{2+} adsorption data fitting the pseudo-first-order and pseudo-second-order model is shown in Fig. 7. As Fig. 7 shown, Pb^{2+} adsorption amount is general increase as adsorption time increases. Pb^{2+} adsorption on MgAl-LDO quickly reaches the adsorption equilibrium before 80 min due to fact that MgAl-LDO has lots of active site. Subsequently, Pb^{2+} adsorption on MgAl-LDO is slow increase. It can be explained that the active sites of MgAl-LDO are occupied and little active site is available for Pb^{2+} adsorption. R^2 value of the pseudo-first-order is low compared to the pseudo-second-order of 0.984. This result indicates that Pb^{2+} adsorption behavior conforms the pseudo-second-order model. The calculated values of qe and qcal are close to the adsorption result based on pseudo-second-order. Therefore, Pb^{2+} adsorption on MgAl-LDO can be more accurately analyzed by the pseudo-second-order (Li et al., 2022).

3.2.2.2. Pb^{2+} adsorption isotherm. Two kinds of adsorption isotherm models such as Langmuir and Freundlich models are used to analyze Pb^{2+} adsorption on MgAl-LDO. Pb^{2+} adsorption data fitting the adsorption isotherm models is listed in the Table 4. As Table 4 shown, the R^2 values of the Langmuir and Freundlich models are 0.975–0.987 and 0.991–0.997, respectively. This result demonstrates that Freundlich model better describes Pb^{2+} adsorption process than Langmuir model. Due to large size of Pb ion, only a small amount of Pb ion can enter the interlayer, and most of the Pb ion are adsorbed on the surface of the hydrotalcite nanosheet. The Pb^{2+} adsorption amount of the MgAl-LDO is 147.89 mg/g, according to Langmuir model calculation. Pb^{2+} adsorption amount of MgAl-LDO is increase as adsorption temperature increases, indicating that Pb^{2+} adsorption on LDO is endothermic process. The fitting result of the adsorption isotherm models is shown in Fig. 8. Table S4 lists the adsorption capacity of similar adsorbents for Pb^{2+} removal from wastewater. The comparison result indicates that MgAl-LDO has promising potential in Pb^{2+} wastewater treatment.

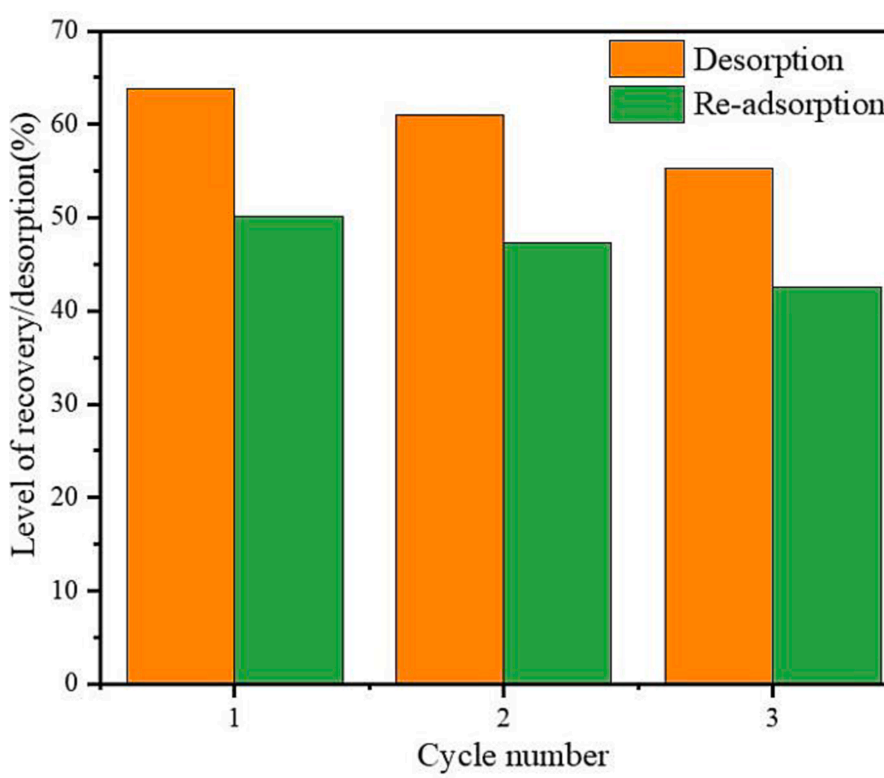

Fig. 11. Desorption-adsorption cycle of the MgAl-LDO.

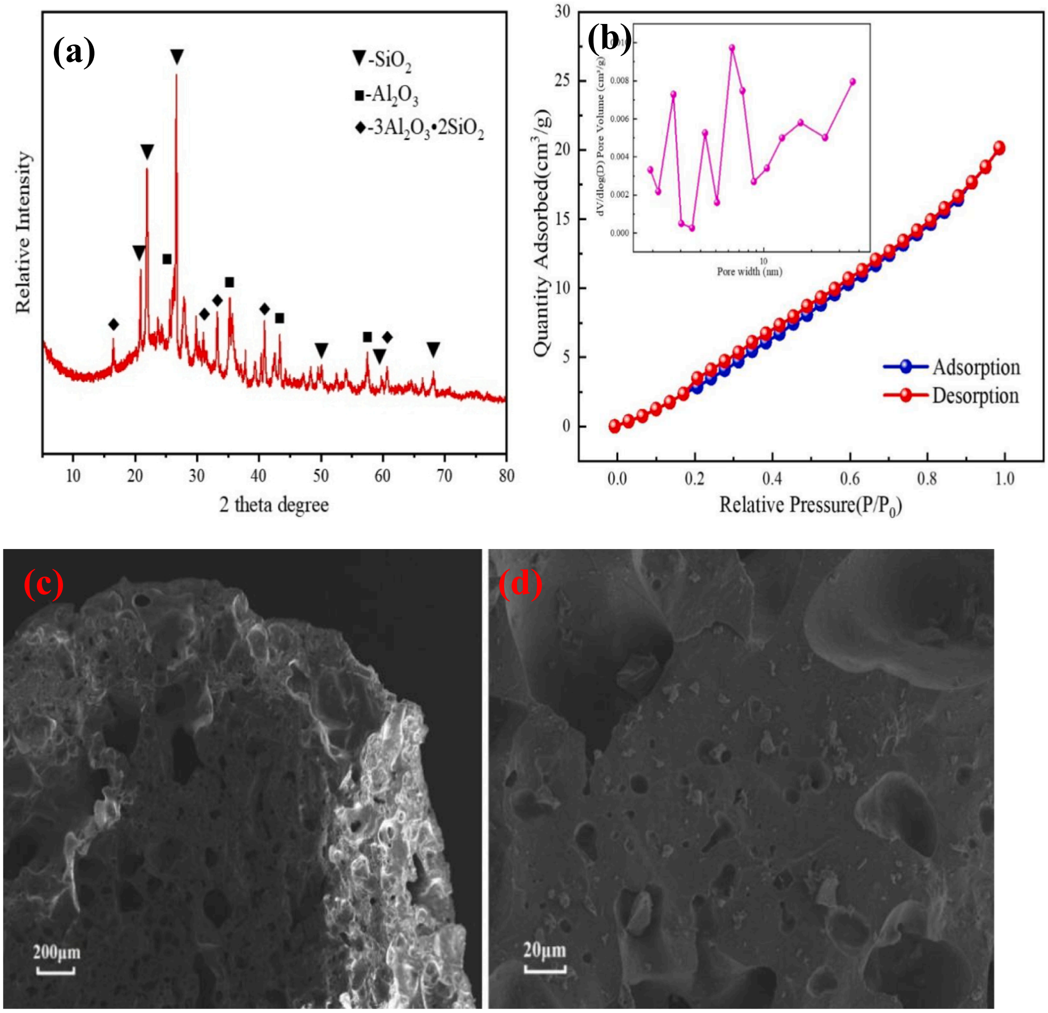

Fig. 12. XRD spectrum of sludge ceramsite (a), N_2 adsorption–desorption isotherms and pore size distribution curves of sludge ceramsite (b), SEM images of sludge ceramsite (c–d).

3.2.2.3. Adsorption mechanism. XRD spectra of the MgAl-LDO before and after Pb^{2+} adsorption are shown in Fig. 9a. As Fig. 9a shown, the characteristic peaks of the MgAl-LDO are weakened after Pb^{2+} adsorption. Besides, the characteristic peaks of $Pb_3(CO_3)_2(OH)_2$ appear at 9.846°, 20.884°, 24.640°, 27.080°, 34.155° and 40.396°. This result indicates that Pb^{2+} forms carbonate precipitation, realizing Pb(II) removal from wastewater. Zhang and Yuntao (2018) reported that Pb^{2+} forms the $Pb_3(CO_3)_2(OH)_2$ on the biochar/hydrotalcite composite, which is similar with our work.

As Fig. 9b-–e– shown, the peaks of the MgAl-LDO before and after Pb^{2+} adsorption almost changed. However, the surface of the MgAl-LDO after Pb^{2+} adsorption is rough, which just likes the "potato chip" shape. The surface of the MgAl-LDO has C, Mg, Al and Pb elements based on EDS mapping images (Fig. 9f–g), indicating that Pb^{2+} is successful adsorbed on the MgAl-LDO.

Fig. 10 shows the XPS spectra of the MgAl-LDO before and after Pb^{2+} adsorption. As shown in Fig. 10a, the sign of the Pb4f is found on the MgAl-LDO after Pb^{2+} adsorption. Besides, Al, Mg, O and C elements are appeared on the MgAl-LDO. The atomic ratio of Mg/Al of the MgAl-LDO decreases from 0.84 to 0.75 after Pb^{2+} adsorption. This result indicates that Mg^{2+} may be replaced with Pb^{2+}, demonstrating that it is existence of cation exchange between Mg^{2+} and Pb^{2+}. Therefore, cation exchange also contributes to Pb^{2+} removal from wastewater. In addition, the spectrum of the C1s has three peaks of the C—C, C—OH and O—C=O groups. However, the peak location and peak area of the C1s spectrum have changed after Pb^{2+} adsorption. For instance, the peak area of C—OH and O—C=O groups decrease by 13.47 % and 5.43 %, respectively. The reason might be that surface oxygen-containing functional groups bond with Pb^{2+} to form O—Pb group, realizing Pb^{2+} removal from wastewater. As Fig. 10d shown, two peaks at 138.17 and 143.02 eV are appeared on the MgAl-LDO after Pb^{2+} adsorption, which are attributed to the $Pb4f_{7/2}$ and $Pb4f_{5/2}$, respectively. This result indicates that it might form the OH—Pb, O—Pb and COO—Pb group, realizing Pb^{2+} removal from wastewater. The Be center of $PbCO_3$ is 138.7 eV, while the Be center of $Pb(OH)_2$ is 137.3 eV based on the report of the Park et al. (2007). The peaks location of the $PbCO_3$ and $Pb(OH)_2$ are within the scope of the 138.17 and 143.02 eV, respectively, indicating Pb^{2+} might form $PbCO_3$ and $Pb(OH)_2$. This result is consistent with XRD analysis. The summary of Pb^{2+} adsorption mechanism is shown in Fig. 10e.

3.2.2.4. Reusability of the MgAl-LDO. The reusability result of the MgAl-LDO is shown in Fig. 11. Thiourea and Pb^{2+} can generate the complex cation $Pb[SC(NH_2)_2]^{2+}$ ($Pb^{2+} + SC(NH_2)_2 = Pb[SC(NH_2)_2]^{2+}$). Therefore, thiourea is used as the desorption agent in the reusability experiment. As Fig. 11 shown, the Pb^{2+} removal decreases after three cycles. The slight decrease of Pb^{2+} removal may be due to the incomplete desorption of Pb^{2+} adsorbed on the MgAl-LDO or the slight destruction of layered structure of MgAl-LDO. The results indicates that MgAl-LDO has good reusability after three cycles.

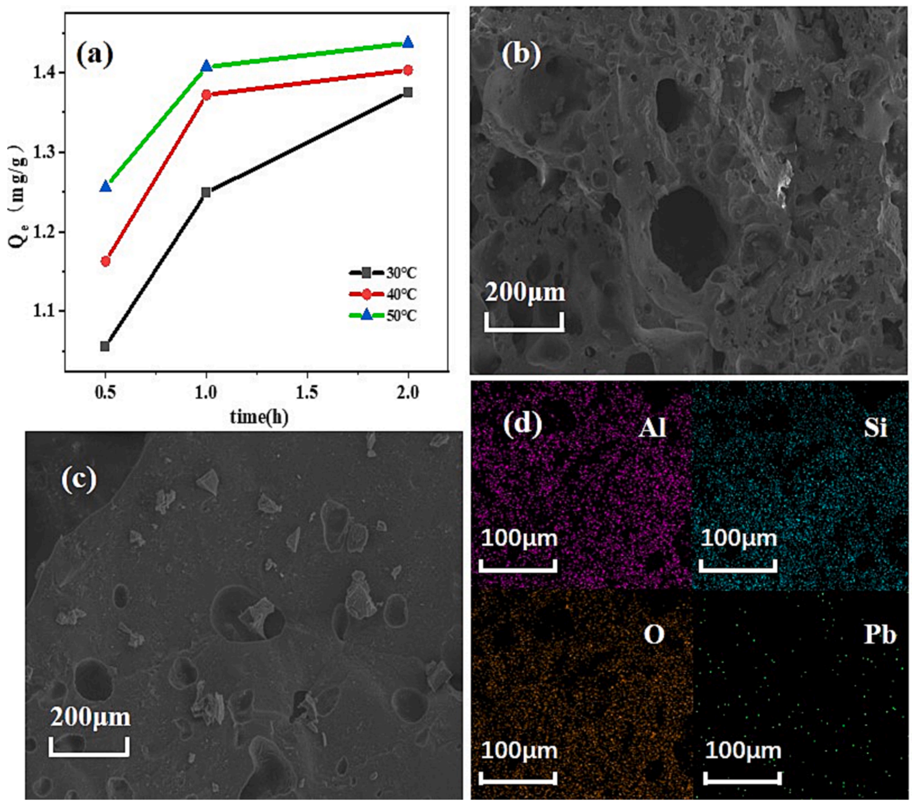

Fig. 13. SEM images of sludge ceramsite (a-b), EDS image of sludge ceramsite adsorption Pb^{2+} (c) and Pb^{2+} adsorption capacity of sludge ceramsite (d).

3.3. Characterization of sludge ceramsite and its application

XRD analysis of the sludge ceramsite is shown in Fig. 12a. As Fig. 12a shown, sludge ceramsite mainly has $3Al_2O_3{\cdot}2SiO_2$, SiO_2 and Al_2O_3 with the high peak intensity. These three minerals constitute the structural skeleton and pore structure of the sludge ceramsite. N_2 adsorption isotherm curve of the sludge ceramsite is shown in Fig. 12b. As Fig. 12b shown, the adsorption isotherm curve of sludge ceramsite belongs to the H3 type, which is the characteristic curve of macroporous solid materials. There is no obvious absorption peak in the low pressure area, and the interaction between sludge ceramsite and nitrogen is weak. A large number of pores of sludge ceramsite are gradually filled by N_2 molecules with increasing in pressure. The N_2 adsorption on the surface of sludge ceramsite generally increases as adsorption pressure increases. Therefore, the N_2 adsorption on sludge ceramsite is multi-layer adsorption with underdeveloped micropores and a large proportion of large pores. The average pore size of the sludge ceramsite is 5.83 nm. The surface of sludge ceramsite is rough, which has lots of the interconnected pores (Fig. 12c–d). Theses pores are formed in the preparation process of the sludge ceramsite.

The adsorption capacity of sludge ceramsite is limited for the wastewater treatment. Therefore, sludge ceramsite is modified to improve its adsorption capacity. The sludge ceramsite is immersed in 1 mol/L sodium hydroxide solution for alkali modification. As Fig. 13a shown, Pb^{2+} adsorption amount of sludge ceramsite after alkali modification is 1.437 mg/g, which is increase with increasing in adsorption temperature. The SEM-EDS images of the sludge ceramsite after Pb^{2+} adsorption are shown in Fig. 13b-–d–. As shown in Fig. 13d, the sludge ceramsite is composed of the Al, Si, O and Pb elements, indicating that Pb^{2+} is successfully adsorbed on the sludge ceramsite.

4. Conclusion

The sludge activated carbon, MgAl-LDO and sludge ceramsite are successfully prepared from sludge for pollutant removal from wastewater. The MO and CIP adsorption on sludge activated carbon can be analyzed using the Langmuir isotherm and pseudo-second-order model with MO adsorption amount of 754.05 mg/g and CIP adsorption amount of 635.62 mg/g, respectively. Mg-Al LDO can quickly remove Pb^{2+} from wastewater with adsorption amount of 147.89 mg/g. Pb^{2+} adsorption mechanism indicates that mineral precipitation and functional group complexation contribute to Pb^{2+} removal from wastewater. Mg—Al LDO also has good reusability after three cycles, which has promising potential in actual application. The prepared sludge ceramsite can be also used as adsorbent for Pb^{2+} wastewater treatment after modification. The Pb^{2+} adsorption ability of the sludge ceramsite should be improved in the future.

Declaration of competing interest

The authors declare that they have no known competing financial interests or personal relationships that could have appeared to influence the work reported in this paper.

Acknowledgments

The authors would like to express their gratitude to the Specialized Research Fund for the National Natural Science Foundation of China (51974110, 52074109, 52274261 and 21966019), Natural Science Foundation of Henan Province (232300420298), the Fundamental Research Funds for the Universities of Henan Province (NSFRF220417) for financial support.

Appendix A. Supplementary material

Supplementary data to this article can be found online at https://doi.org/10.1016/j.arabjc.2024.105671.

References

Awa, S.H., Hadibarata, T., 2020. Removal of heavy Mmtals in contaminated soil by phytoremediation mechanism: a review. Water Air Soil Pollut. 231 (2), 47.

Benalia, M.C., Youcef, L., Bouaziz, M.G., Achour, S., Menasra, H., 2021. Removal of heavy metals from industrial wastewater by chemical precipitation: mechanisms and sludge characterization. Arab. J. Sci. Eng. 47, 5587–5599.

Chakraborty, R., Asthana, A., Singh, A.K., Jain, B., Susan, A.B.H., 2020. Adsorption of heavy metal ions by various low-cost adsorbents: a review. Int. J. Environ. Anal. Chem. 102, 342–379.

Cheng, S., Xing, B., Shi, C., Nie, Y., Xia, H., 2021a. Efficient and selective removal of Pb (II) from aqueous solution by modification crofton weed: experiment and density functional theory calculation. J. Clean. Prod. 280, 124407.

Cheng, S., Liu, Y., Xing, B., Qin, X., Zhang, C., Xia, H., 2021b. Lead and cadmium clean removal from wastewater by sustainable biochar derived from poplar saw dust. J. Clean. Prod. 314, 128074.

Cheng, H., Liu, Y., Li, X., 2021c. Adsorption performance and mechanism of iron-loaded biochar to methyl orange in the presence of Cr6+ from dye wastewater. J. Hazard. Mater. 415, 125749.

Cheng, S., Meng, M., Xing, B., Shi, C., Nie, Y., Xia, D., Yi, G., Zhang, C., Xia, H., 2022a. Preparation of valuable pyrolysis products from poplar waste under different temperatures by pyrolysis: evaluation of pyrolysis products. Bioresour. Technol. 364, 128011.

Cheng, S., Zhao, S., Xing, B., Shi, C., Meng, W., Zhang, C., Bo, Z., 2022b. Facile one-pot green synthesis of magnetic separation photocatalyst-adsorbent and its application. J. Water Process Eng. 47, 102802.

Dabrowski, A., Hubicki, Z., Podkościelny, P., Robens, E., 2004. Selective removal of the heavy metal ions from waters and industrial wastewaters by ion-exchange method. Chemosphere 56, 91–106.

Florent, M., Policicchio, A., Niewiadomski, S., Bandosz, T.J., 2019. Exploring the options for the improvement of H_2S adsorption on sludge derived adsorbents: building the composite with porous carbons. J. Clean. Prod. 249, 119412.

Foroutan, R., Peighambardoust, S.J., Ahmadi, A., Akbari, A., Farjadfard, S., Ramavandi, B., 2021. Adsorption mercury, cobalt, and nickel with a reclaimable and magnetic composite of hydroxyapatite/Fe_3O_4/polydopamine. J. Environ. Chem. Eng. 9 (4), 105709.

Foroutan, R., Mohammadi, R., Ahmadi, A., Bikhabar, G., Babaei, F., Ramavandi, B., 2022. Impact of ZnO and Fe_3O_4 magnetic nanoscale on the methyl violet 2B removal efficiency of the activated carbon oak wood. Chemosphere 286, 131632.

Hu, J., Zhao, L., Luo, J., Gong, H., Zhu, N., 2022. A sustainable reuse strategy of converting waste activated sludge into biochar for contaminants removal from water: modifications, applications and perspectives. J. Hazard. Mater. 438, 129437.

Jawad, A., Peng, L., Liao, Z., Zhou, Z., Shahzad, A., Ifthikar, J., Zhao, M., Chen, Z., Chen, Z., 2018. Selective removal of heavy metals by hydrotalcites as adsorbents in diverse wastewater: different intercalated anions with different mechanisms. J. Clean. Prod. 211, 1112–1126.

Khatem, R., Miguel, R.O., Bakhti, A., 2015. Use of synthetic clay for removal of diclofenac anti-inflammatory. Eur. J. Soil. 4 (2), 126–136.

Le, Y., He, X., Liu, M., Liu, X., Zhou, S., Xie, R., Fu, Y., Wang, H., Sun, J., 2023. Light-driven sustainable enhancement of Cr(VI) reduction via the combination of Cr(VI)-reducing bacteria, *Paraclostridium bifermentans* with CdS nanoparticles. J. Environ. Chem. Eng. 11 (5), 110364.

Lee, M.E., Park, J.H., Chung, J.W., 2019. Comparison of the lead and copper adsorption capacities of plant source materials and their biochars. J. Environ. Manage. 236, 118–124.

Li, X., Zeng, G.M., Huang, J.H., Zhang, C., Fang, Y.Y., Qu, Y.H., Luo, F., Lin, D., Liu, H.L., 2009. Recovery and reuse of surfactant SDS from a MEUF retentate containing Cd2+ or Zn2+ by ultrafiltration. J. Membr. Sci. 337, 92–97.

Li, X., Shi, J., Luo, X., 2022a. Enhanced adsorption of rhodamine B from water by Fe-N co-modified biochar: preparation, performance, mechanism and reusability. Bioresour. Technol. 343, 126103.

Li, X., Xu, J., Luo, X., Shi, J., 2022b. Efficient adsorption of dyes from aqueous solution using a novel functionalized magnetic biochar: synthesis, kinetics, isotherms, adsorption mechanism, and reusability. Bioresour. Technol. 360, 127526.

Liu, H., Xu, G., Li, G., 2021. Preparation of porous biochar based on pharmaceutical sludge activated by NaOH and its application in the adsorption of tetracycline. J. Colloid Interface Sci. 587, 271–278.

Ma, Y., Li, P., Yang, L., Wu, L., He, L., Gao, F., Qi, X., Zhang, Z., 2020. Iron/zinc and phosphoric acid modified sludge biochar as an efficient adsorbent for fluoroquinolones antibiotics removal. Ecotoxicol. Environ. Saf. 196, 110550.

Omer, A.M., Abd El-Monaem, E.M., Eltaweil, A.S., 2022. Novel reusable amine-functionalized cellulose acetate beads impregnated aminated graphene oxide for adsorptive removal of hexavalent chromium ions. Int. J. Biol. Macromol. 208, 925–934.

Park, M., Choi, C.L., Seo, Y.J., Yeo, S.K., Choi, J., Komarneni, S., Lee, J.H., 2007. Reactions of Cu2+ and Pb2+ with Mg/Al layered double hydroxide. Appl. Clay Sci. 37 (1), 143–148.

Qin, X., Tao, R., Cheng, S., Xing, B., Meng, W., Nie, Y., Zhang, C., Yu, J., 2024. Microwave-assisted one-pot method preparation of ZnO decorated biochar for levofloxacin and Cr(VI) removal from wastewater. Ind. Crop. Prod. 208, 117863.

Qu, X., Jeon, S., Jeong, J., Kang, W., Xing, B., Zhang, C., Hong, S.W., 2023a. In situ grown core/shell heterostructure of $CuCo_2O_4$/NiCo-LDH composite intercalated by glucose on Ni networks for all-solid-state hybrid supercapacitor electrodes. J. Storage Mater. 73, 108540.

Qu, X., Kwon, Y.W., Jeon, S., Jeong, J., Kang, W., Jiang, Z., Zhang, C., Hong, S.W., 2023b. Foldable and wearable supercapacitors for powering healthcare monitoring applications with improved performance based on hierarchically co-assembled CoO/NiCo networks. J. Colloid Interface Sci. 634, 715–729.

Ran, B., De, Y., Bin, L., Feifei, C., Ran, Z., Wei, L., 2022. Mercaptocarboxylic acid intercalated MgAl layered double hydroxide adsorbents for removal of heavy metal ions and recycling of spent adsorbents for photocatalytic degradation of organic dyes. Sep. Purif. Technol. 289, 120741.

Shi, J., Huang, W., Han, H., Xu, C., 2021. Pollution control of wastewater from the coal chemical industry in China: environmental management policy and technical standards. Renew. Sustain. Energy Rev. 143, 110883.

Shi, F., Xing, B., Zeng, H., Guo, H., Qu, X., Huang, G., Cao, Y., Li, P., Feng, L., Zhang, C., 2024. Facile synthesis of ultrathin carbon nanosheets through NaCl-KCl templates coupled with ice-induced assembly strategy from carbon quantum dots as lithium-ion batteries anodes. J. Alloys Compd. 976, 173325.

Song, B., Xia, D., Guo, H., Dong, Z., Wang, Y., Zhao, W., Chen, Z., 2023. Effect of fat, oil and grease (FOG) on the conversion of lignite to biogenic methane. Fuel 331, 125367.

Vázquez-Durán, A., Nava-Ramírez, M.J., Téllez-Isaías, G., Méndez-Albores, A., 2022. Removal of aflatoxins using agro-waste-based materials and current characterization techniques used for biosorption assessment. Front. Vet. Sci. 9, 897302.

Wang, H., Le, Y., Sun, J., 2022a. Consolidated bioprocessing of biomass and synthetic cadmium wastewater substrates for enhancing hydrogen production by *Clostridium thermocellum*-CdS complex. Fuel 316, 123207.

Wang, H., Le, Y., Sun, J., 2022b. Light-driven bio-decolorization of triphenylmethane dyes by a clostridium thermocellum-CdS biohybrid. J. Hazard. Mater. 431, 128596.

Wang, H., Liu, R., Chen, Q., Mo, Y., Zhang, Y., 2022c. Biochar-supported starch/chitosan-stabilized nano-iron sulfide composites for the removal of lead ions and nitrogen from aqueous solutions. Bioresour. Technol. 347, 126700.

Yan, J., Zuo, X., Yang, S., Chen, R., Cai, T., Ding, D., 2022. Evaluation of potassium ferrate activated biochar for the simultaneous adsorption of copper and sulfadiazine: competitive versus synergistic. J. Hazard. Mater. 424, 127435.

Yuan, Q., Zhang, H., Qin, C., Zhang, H., Wang, D., Zhang, Q., Zhang, D., Zhao, J., 2023. Impact of emerging pollutant florfenicol on enhanced biological phosphorus removal process: focus on reactor performance and related mechanisms. Sci. Total Environ. 859, 160316.

Yurak, V., Apakashev, R., Dushin, A., Usmanov, A., Lebzin, M., Malyshev, A., 2021. Testing of natural sorbents for the assessment of heavy metal ions' adsorption. Appl. Sci. 11 (8), 3723.

Zeng, H., Xing, B., Zhang, C., Nie, Y., Qu, X., Xu, B., Huang, G., Sun, Q., Cao, Y., Won Hong, S., 2023. Edge-boron-functionalized coal-derived graphite nanoplatelets prepared via mechanochemical modification for enhanced Li-ion storage at low-voltage plateau. Appl. Surf. Sci. 621, 156870.

Zhang, H., Zhao, J., Fu, Z., Wang, Y., Guan, D., Xie, J., Zhang, Q., Liu, Q., Wang, D., Sun, Y., 2023. Metagenomic approach reveals the mechanism of calcium oxide improving kitchen waste dry anaerobic digestion. Bioresour. Technol. 387, 129647.

Zhang, X.G., Yuntao, 2018. Simultaneous and efficient capture of inorganic nitrogen and heavy metals by polyporous layered double hydroxide and biochar composite for agricultural nonpoint pollution control. ACS Appl. Mater. Interfaces 10 (49), 43013–43030.

Zhao, J., Zhang, H., Guan, D., Wang, Y., Fu, Z., Sun, Y., Wang, D., Zhang, H., 2023. New insights into mechanism of emerging pollutant polybrominated diphenyl ether inhibiting sludge dark fermentation. Bioresour. Technol. 368, 128358.

Zhou, R., Zhang, M., Shao, S., 2022. Optimization of target biochar for the adsorption of target heavy metal ion. Sci. Rep. 12, 13662.